Desalination and Water Treatment
www.deswater.com

doi:10.5004/dwt.2019.23487

141 (2019) 256–268
February

Preparation and evaluation of granular Fe-impregnated attapulgite adsorbents (Fe-ATP) for arsenic removal from contaminated groundwater

Bai Sun[a,b,*], Hui Wang[a], Chen-Feng Ding[a], Yu-Xian Guo[c], Shu-Guang Zhu[a], Jin Zhang[a], Ling-Tao Kong[b,*]

[a]*Key Laboratory of Water Pollution Control and Wastewater Resource of Anhui Province, College of Environment and Energy Engineering, Anhui Jianzhu University, Hefei, 230601, China, Tel. +86-551-65591132, Fax +86-551-65592420, email: bsun@mail.ustc.edu.cn (B. Sun), 837104889@qq.com (H. Wang), 838842021@qq.com (C.-F. Ding), 286537056@qq.com (S.-G. Zhu), ginnzy@163.com (J. Zhang)*

[b]*Nano-materials and environmental detection laboratory, Hefei Institute of Physical Science, Chinese Academy of Sciences, Hefei, 230031, China, email: ltkong@iim.ac.cn (L.-T. Kong)*

[c]*College of Mathematics and Physics, Anhui Jianzhu University, Hefei, 230601, China, email: guo_yuxian@163.com (Y.-X. Guo)*

Received 5 May 2018; Accepted 18 November 2018

ABSTRACT

Granular iron-impregnated attapulgite adsorbents (Fe-ATP) were developed for effective removal of arsenic from groundwater. Fe-ATP with an iron content of 15% and calcinated at temperature of 200°C showed the best adsorption performance for both arsenite and arsenate. The adsorption data of arsenite onto Fe-ATP fitted both Langmuir and Freundlich isotherms well, while Langmuir described the adsorption of arsenate onto Fe-ATP better than Freundlich isotherm. Both arsenite and arsenate adsorption onto Fe-ATP followed pseudo-second-order kinetics model. The removal efficiency of arsenite by Fe-ATP was insensitive to pH in a wide pH range of 3–11, however, Fe-ATP exhibited better removal performance for arsenate in the pH < 7 conditions. Co-existing anions did not evidently inhibit arsenic removal by Fe-ATP. In column tests using lab-prepared arsenic containing water as influent, about 4900, 1500 and 550 (1320, 520 and 260) bed volumes (BVs) of water with 200 μg/L arsenite (arsenate) were treated before breakthrough (10 μg/L, WHO standard) was reached under flowing rates of 200, 600 and 1000 mL/h, respectively. While the influent contaminant concentration was 303 μg/L from real groundwater and the flowing rate was 200 mL/h, breakthrough BVs at the WHO provisional guideline value of 10 μg/L were 1300.

Keywords: Arsenite; Arsenate; Adsorption; Iron; Attapulgite

1. Introduction

Attapulgite (ATP) is a crystalline hydrated magnesium aluminum silicate with unique three-dimensional structures and has a fibrous morphology [1–4]. ATP, abundant in nature, is cheap and easily available. One of the distinctive features of ATP is its good adsorption property for many chemical substances, which derives mainly from its high specific surface area, abundant silanol groups on its surfaces and cation exchange capacity [1–3]. ATP has permanent negative charges on its surface, which enable it to adsorb cationic contaminants. In last decades, ATP has been intensively investigated as adsorbent in the removal of cationic organic contaminants, heavy metal ions and radionuclide from the water [1,3,5,6]. However, a few investigators have conducted research on the adsorption of anions by ATP-based adsorbents [7,8], since natural ATP with permanent negative charges repulses anions.

Arsenic has been ranked as a high priority top 20 hazardous substances by the Agency for Toxic Substances and Disease Registry (ATSDR) [9,10]. Among the various forms of arsenic, As(III) and As(V) are responsible for groundwa-

*Corresponding author.

ter contamination, and As(III) has greater toxicity and more mobility compared to As(V) [10–12]. Long-term ingestion of high levels of arsenic-contaminated drinking water, over the maximum contaminant level (MCL) of 0.01 mg/L set by the World Health Organization (WHO) causes dermal problems, headaches, vomiting, cancers in different organs and, even death [13–16]. Studies have revealed that iron(III) has a high affinity toward inorganic arsenic species, and it is very selective to arsenic in the adsorption process [8,11,16,17]. Considering the affinity of arsenic toward iron, various iron-based adsorbents have been developed and effectively used for removing both As(III) and As(V) from contaminated water [14,17,18]. Since the fine powdery form of iron oxides hinders their separation from the aqueous solution, iron has been impregnated or loaded into various porous carriers such as activated carbon, diatomite, polymer, and so on [11,15,16,19–21]. However, to the best of our knowledge, ATP has rarely been used as carrier for iron impregnation in removal of arsenic. On the other hand, most reported adsorbents exhibited poor adsorption performance for As(III) which is more prevalent and toxic than As(V) in groundwater. Some pretreatment processes including the oxidation of As(III) to As(V) are needed which results not only in higher run cost but also in more complex operation.

In this work, Fe(III) was loaded into ATP using the wet impregnation process. Fe-ATP adsorbents with different iron content and calcinated at different temperatures were prepared. Arsenic removal potential of the Fe-ATP adsorbent was systematically investigated under various operating conditions such as initial arsenic concentration, pH, contact time and co-existing anions. Fe-ATP showed excellent removal performance for both As(III) and As(V). Furthermore, arsenic removal performance of Fe-ATP was evaluated for lab-prepared arsenic-containing water and real arsenic-contaminated groundwater samples using column tests.

2. Materials and methods

2.1. Materials

All the chemicals used in this study were purchased from Sinopharm Chemical Reagent Co., Ltd., Shanghai, China with analytical reagent grade. ATP was purchased from Mingguang Xingxin Mineral Co., Ltd., China. The ATP was first washed with distilled water for several times and then dried at 105°C for 12 h to eliminate the free water. As(III) and As(V) stock solutions were prepared by dissolving Na_3AsO_3 and Na_3AsO_4, respectively, in distilled water.

2.2. Granular Fe-ATP adsorbent preparation

The granular Fe-ATP adsorbent was prepared in a two-step process. (1) Powder preparation: Positive ferric ions were loaded on the ATP surface by coordination reactions between ferric ions and silanol/aluminol groups using the wet impregnation method. Briefly, 100 g dried ATP was first added into 1 L doubly distilled water to obtain a homogeneous suspension. Then, a certain quality ratio of $Fe(NO_3)_3$ was added into the suspension. After stirring for two hours, the mixture was mixed with a certain amount of NaOH under vigorous stirring until the pH was stabilized at 7.5. Stirring for another 2 h, the resulting suspensions were washed repeatedly with doubly distilled water until the supernatant pH was neutral. Next, the suspension was filtrated and dried at 80°C for 24 h. (2) Granulation: The Fe-ATP powder was adequately blended in a dispersion kneader and then transferred into an extrusion machine to obtain strip-like adsorbent under a pressure of about 6 MPa. These strips were then calcinated at 200, 250, and 300°C for 2 h in a muffle furnace. Finally, the calcinated strips were manually broken into desired lengths.

2.3. Adsorbent characterizations and chemical analysis

The X-ray diffraction (XRD) patterns of the adsorbents were performed on a D/MaxIIIA X-ray diffractometer (Rigaku Co., Japan), using Cu Kα ($\lambda_{K\alpha1}$ = 1.5418 Å) as the radiation source in the range of 5–80°. Scanning electron microscopy (SEM) image of the adsorbent was obtained with a FEI Quanta 200 FEG field emission scanning electron microscope. The energy dispersive spectrum (EDS) and elemental mapping were performed on a Zeiss Auriga microscope equipped with an Oxford Inca X-Max 50 detector. The Fourier transform infrared (FT-IR) spectra of the adsorbents before and after adsorption were recorded with a NEXUS-870 FT-IR spectrometer in the range of 4000–400 cm^{-1}. The Brunauer, Emmett, and Teller (BET) specific surface area and pore volume of the adsorbent were determined by BET N_2 adsorption-desorption analysis using a Micromeritics ASAP2000 surface area analyzer (Norcross, USA). The As(III) and As(V) concentrations were determined in the liquid phase using inductively coupled plasma mass spectrometry (ICP-MS, Thermo Fisher Scientific model iCAPRQ). The zeta potentials were measured by zeta potentiometer (microtrac model zetacheck).

2.4. Batch adsorption experiments

Batch adsorption experiments were carried out in a thermostatic shaker at room temperature and shaking speed of 150 rpm. After a period of adsorption was carried out, the adsorbents were filtrated and the solution was collected for arsenic measurement.

The adsorption isotherm studies were carried out by varying initial concentrations of arsenic under a fixed Fe-ATP dose of 2.5 g/L, with a total volume of 20 mL in 50 mL polyethylene bottles. The pH was adjusted by adding aqueous solutions of 0.1 M HCl or 0.1 M NaOH. After a period of 24 h, residual arsenic in the solution was analyzed. In the study of pH effect on arsenic adsorption, 50 mg of Fe-ATP was added into 20 mL of arsenic solution with a concentration of 5 mg/L and the pH was adjusted and maintained at a specified value in the range of 3–11. The adsorption kinetics was determined by an analysis of the adsorption capacity at different time intervals. In kinetics study, 150 mg of Fe-ATP were added to 150 mL of arsenic solution with a concentration of 1 mg/L at neutral pH. At predetermined time intervals, stirring was interrupted while 6 mL of supernatant solutions were pipetted and filtrated for the determination of the remaining arsenic concentrations. The effects of co-existing anions (HCO_3^-, SO_4^{2-},

PO_4^{3-}, Cl^- and NO_3^-) on arsenic adsorption were also investigated. The pH was fixed at neutral and the Fe-ATP dose was 2.5 g/L.

Adsorption experiments were carried out in duplicate and the average data were used to evaluate the adsorption performance. Adsorption capacity was calculated from the relationship:

$$q_e = \frac{(C_0 - C_e)\,V}{m} \tag{1}$$

where q_e (mg/g) is the equilibrium adsorption capacity, C_0 and C_e represent the initial and equilibrium arsenic concentrations (mg/L), V (L) is the volume of solution and m (g) is the weight of the adsorbent.

Experimental data for arsenic adsorption isotherm studies were fitted with a Langmuir or a Freundlich model as expressed by Eqs. (2) and (3), respectively.

$$\frac{C_e}{q_e} = \frac{1}{q_m K_L} + \frac{C_e}{q_m} \tag{2}$$

$$\ln q_e = \frac{1}{n}\ln C_e + \ln K_F \tag{3}$$

where q_m and K_L are Langmuir constants, representing the maximum adsorption capacity of adsorbents (mg/g) and the energy of adsorption, respectively. K_F and n are Freundlich constants related to adsorption capacity and adsorption intensity, respectively.

Experimental data for the arsenic kinetics adsorption studies were fitted with a pseudo second order kinetic model as expressed by Eq. (4).

$$\frac{t}{q_t} = \frac{1}{k_2 q_e^2} + \frac{1}{q_e}t \tag{4}$$

where q_e and q_t are the amount of arsenic adsorbed at equilibrium and at time t, respectively. k_2 is the rate constant of the pseudo-second-order model of adsorption (g/mg/min).

2.5. Column experiments

Fixed bed column study was conducted using borosilicate glass columns of 4 cm internal diameter. The column was packed with Fe-ATP of 15 cm length between two supporting layers of glass wool (~3 cm) to prevent the adsorbent floating from the outlet. Two kinds of water, lab-prepared arsenic-containing water and arsenic-contaminated groundwater, were used as the feed solution. The columns were operated at influent arsenic flowing rates of 200, 600, and 1000 mL/h,and the corresponding empty bed contact time (EBCT) were 56.5, 18.8, and 11.3 min, respectively. The effluent was collected at regular intervals and the concentrations of arsenic were measured.

Results and discussions

3.1. Characterization of Fe-ATP

Fig. 1 shows the photograph and SEM image of Fe-ATP with iron loading of 15% and calcinated at 200°C. The prepared Fe-ATP granular adsorbents are 1.2–1.6 mm in diameter and 2–6 mm in length, as shown in Fig. 1a. Fig. 1b reveals that the adsorbent is the aggregation of some nanoscale materials and the surface of it is porous. This kind of structural properties is expected to result in a high adsorption performance for toxic anions. To examine the iron oxide phase impregnated into ATP, all the samples were detected by XRD. The XRD patterns of typical unmodified ATP and Fe-impregnated ATP calcinated at 200°C with a Fe content of 15% are shown in Fig. 2. It can be seen from Fig. 2 that the diffraction peaks of ATP still exist after Fe impregnation indicating that the ATP structure was not destroyed in the synthesis of Fe-ATP. The XRD pattern of Fe-ATP reveals a hematite phase indicated by peaks at 2θ = 56.7°. Quartz, montmorillonite and aluminum oxide were also identified in the XRD pattern and have been marked in Fig. 2. A sharp peak for aluminum oxide become obvious after Fe loading and calcination at 2θ = 45.7°.

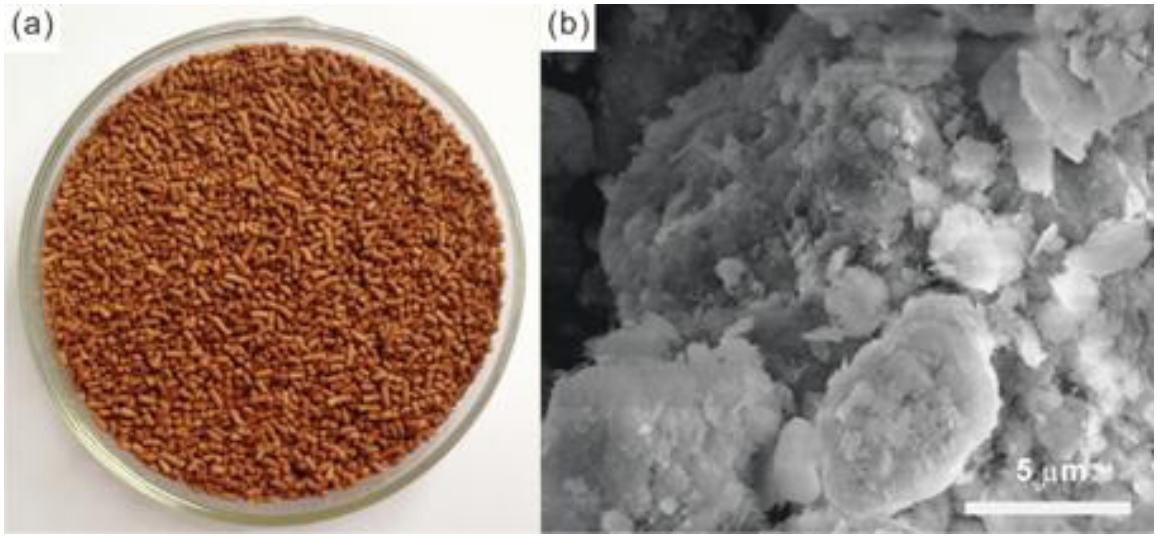

Fig. 1. (a) Photograph of granular Fe-ATP adsorbent; (b) SEM image of the surface of the Fe-ATP. (Fe loading: 15%; calcination temperature: 200°C).

The EDS spectrum and elemental mapping images of Fe-ATP are shown in Fig. 3. In Fig. 3a, the signals of Fe, Al, Si and O can be observed, indicating that iron has been loaded onto the Fe-ATP. Moreover, the elemental mapping images of Fe, Al, Si and O demonstrate that each element is homogeneously distributed within the Fe-ATP. Fig. 3b shows the selected scan area of Fe-ATP in the elemental mapping.

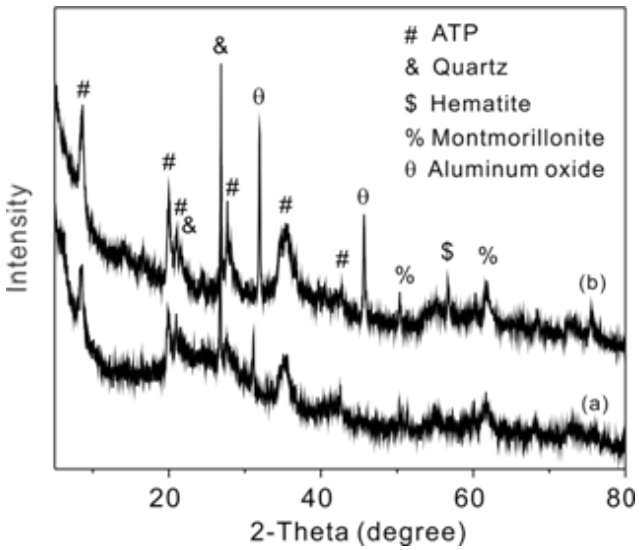

Fig. 2. XRD patterns of (a) un-modified and (b) iron-impregnated ATP.

3.2. Adsorption isotherms

To investigate the adsorption capacity of Fe-ATP, the arsenic adsorption isotherms for different samples were studied (Fig. 4). The equilibrium data were fitted using Langmuir and Freundlich isotherm models (Figs. 5 and 6) and the corresponding fitting results are shown in Table 1. Figs. 4a,c show the adsorption isotherms of arsenite and arsenate on Fe-ATP calcinated at different temperatures at pH 7.0. In this case, the iron loading was maintained at 15%. For arsenite, the adsorption data fitted both Langmuir and Freundlich isotherms well ($R^2 > 0.97$). With the increase of post-treatment temperature, the adsorption performance of the samples for both arsenite and arsenate became poor. As the calcination temperature increased from 200 to 300°C, the maximum adsorption capacity for arsenite decreased from 23.47 to 16.42 mg/g. For arsenate, the adsorption data fitted Langmuir isotherm better than Freundlich isotherm. Also, when the post-treatment temperature increased the adsorption capacities for arsenate decreased (Table 1). Next, we investigate the influence of different iron loadings on the performance of arsenite and arsenate adsorption. The adsorption isotherms of arsenite and arsenate on Fe-ATP with different iron loadings at pH 7.0 are shown in Figs. 4b,d. The linear fitting curves and fitting results can be found in Fig. 6 and Table 1. We found that the adsorption capacity of the samples for arsenic was not proportional to the loading of iron. For both arsenite and arsenate, the adsorption performance first increased and then decreased as the iron loading increased from 5 to 50%. And the best adsorption performance for both arsenite and arsenate was the iron loading of 15%. For all the iron loadings, arsenite adsorption data fitted both Langmuir and Freundlich iso-

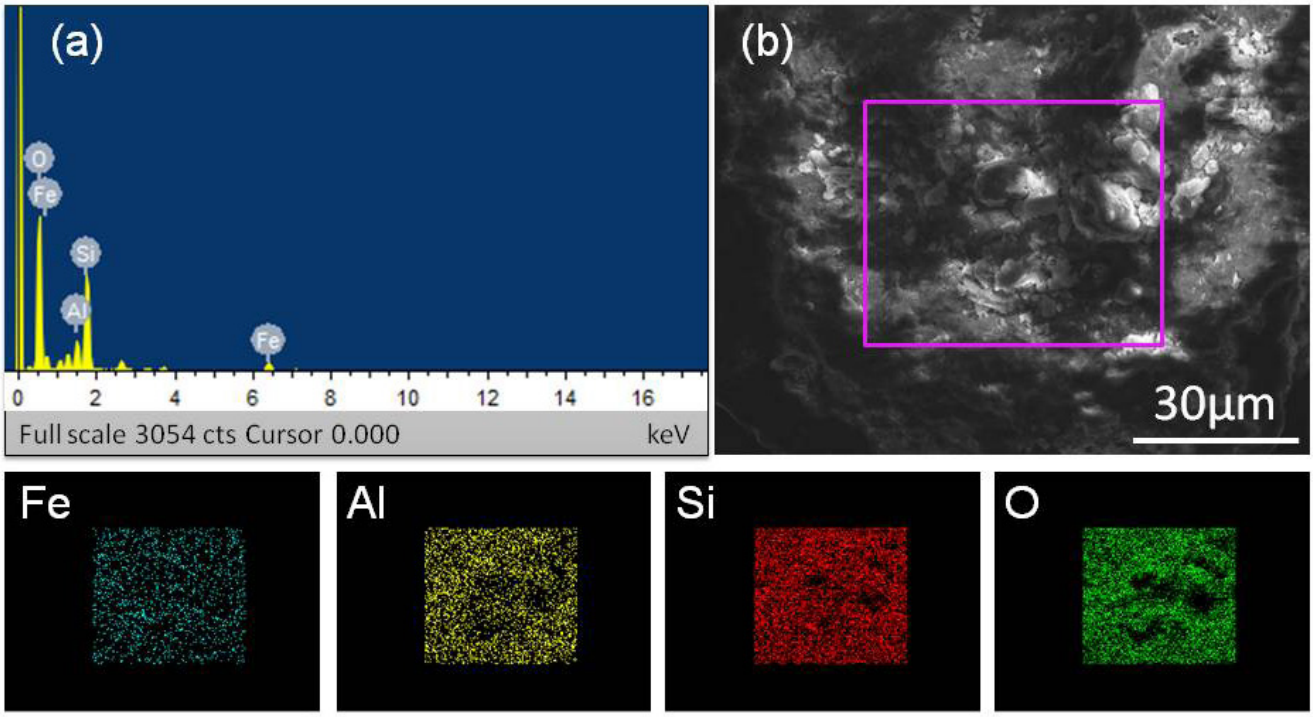

Fig. 3. The EDS spectrum and elemental mapping images of Fe-ATP.

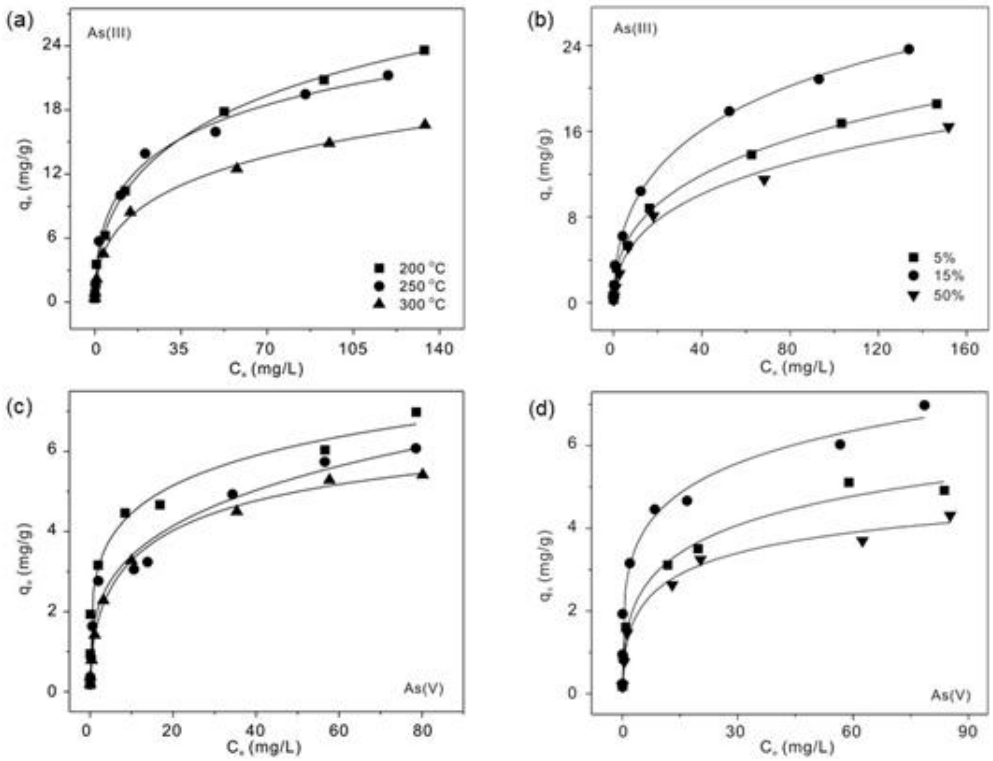

Fig. 4. Adsorption isotherms of (a) arsenite and (c) arsenate on Fe-ATP calcinated at different temperatures, (b) arsenite and (d) arsenate on Fe-ATP with different iron loadings.

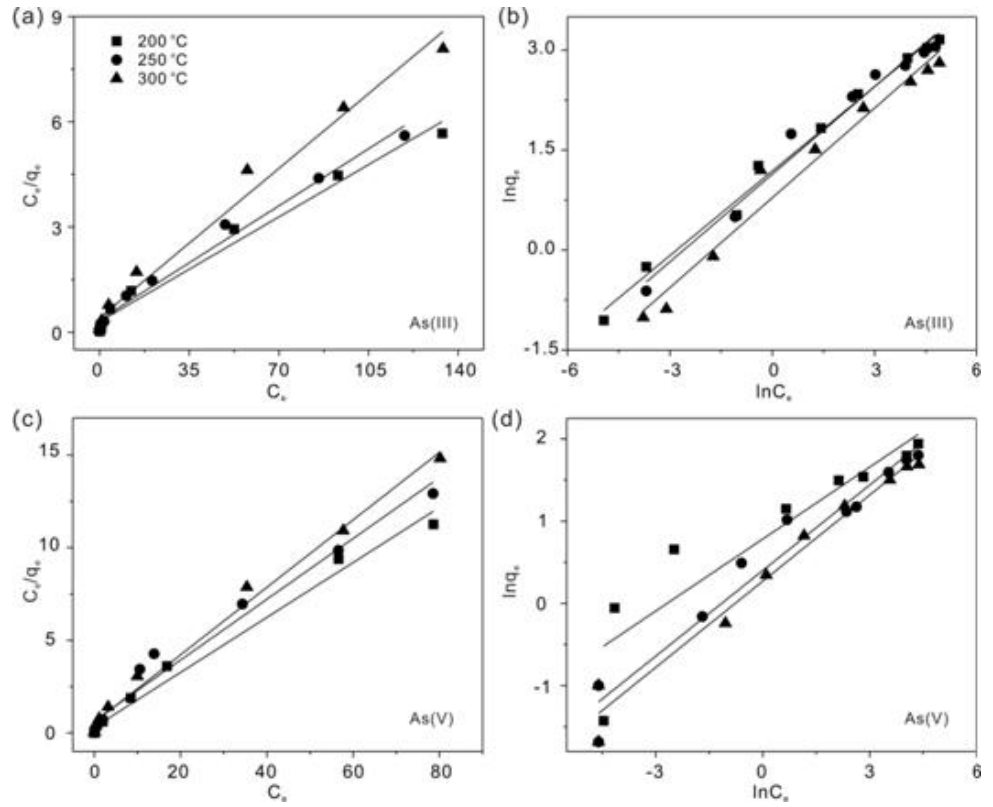

Fig. 5. Linear Langmuir and Freundlich fitted curves of As(III) (a, b) and As(V) (c, d) adsorption onto Fe-ATP prepared calcinated at different temperatures.

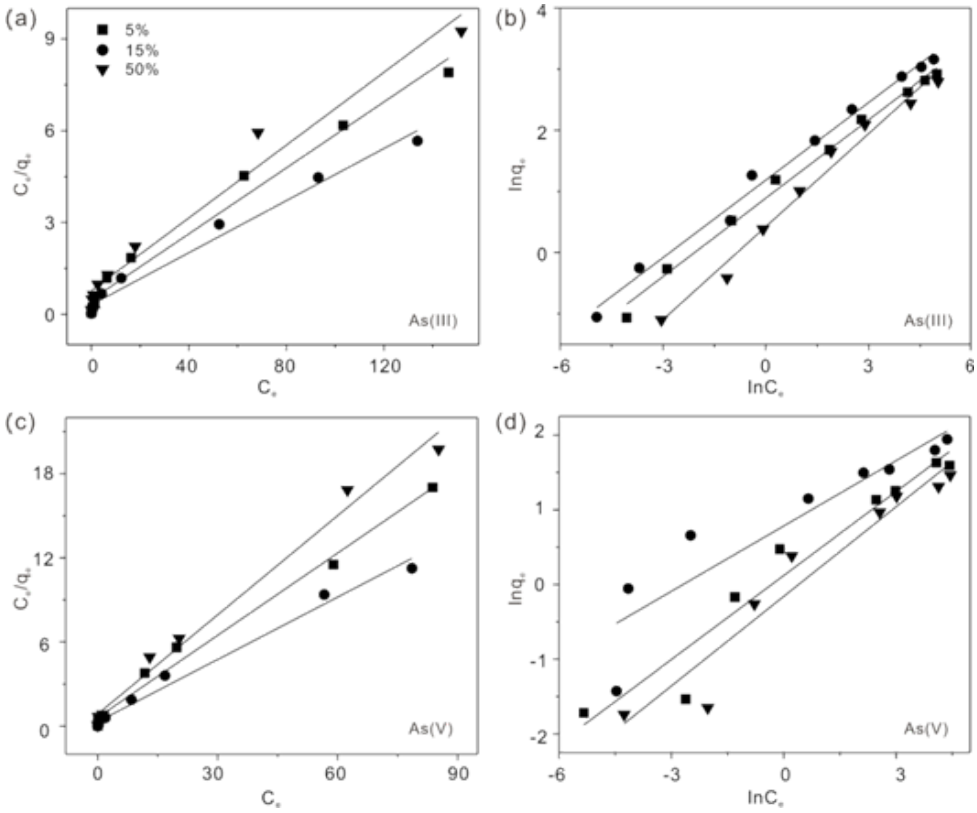

Fig. 6. Linear Langmuir and Freundlich fitted curves of As(III) (a, b) and As(V) (c, d) adsorption onto Fe-ATP with different iron contents.

Table 1
Isotherm fitting for arsenic adsorption onto Fe-ATP with different iron loadings and calcinated at different temperatures

As species	K_L		Langmuir			Freundlich		
			q_m	R^2	K_F	n	R^2	
Arsenite	Temperature[a]	200	0.14	23.47	0.98	3.28	2.36	0.99
	(°C)	250	0.13	21.54	0.98	3.13	2.28	0.97
		300	0.15	16.42	0.98	2.19	2.23	0.97
	Fe content[b]	5	0.11	18.55	0.98	2.44	2.34	0.99
	(%)	50	0.08	16.80	0.97	1.53	1.97	0.98
Arsenate	Temperature[a]	200	0.48	6.74	0.97	1.31	2.87	0.97
	(°C)	250	0.25	6.10	0.98	1.49	2.89	0.95
		300	0.32	5.49	0.99	2.17	3.43	0.82
	Fe content[b]	5	0.32	5.12	0.99	1.13	2.67	0.93
	(%)	50	0.27	4.24	0.99	0.85	2.50	0.92

a, the content of Fe is 15%; b, the calcination temperature is 200°C.

therms reasonably well ($R^2 > 0.96$) and arsenate adsorption data fitted Langmuir isotherm better than Freundlich isotherm. So the calcination temperature of 200°C and the iron loading of 15% are the optimized parameters in our system. It is known that the solute adsorption depends on the surface area and the surface functional groups of the porous adsorbent. So, further BET surface area and FT-IR measurements (in powder form) were performed to investigate the reason for the difference in adsorption capacity of different samples (Figs. 7, 8). And the corresponding parameters are given in Tables 2 and 3. The BET surface areas of the Fe-impregnated ATP are shown in Fig. 7. The surface areas were significantly affected by the calcination temperature and iron content. As the calcination temperature increased the BET surface areas first decreased from 137.6 to 128.8 cm^2/g and then increased to 137.8 cm^2/g and the total volume and average pore size did not change a lot. With the increasing of Fe content, both the surface areas and total volumes

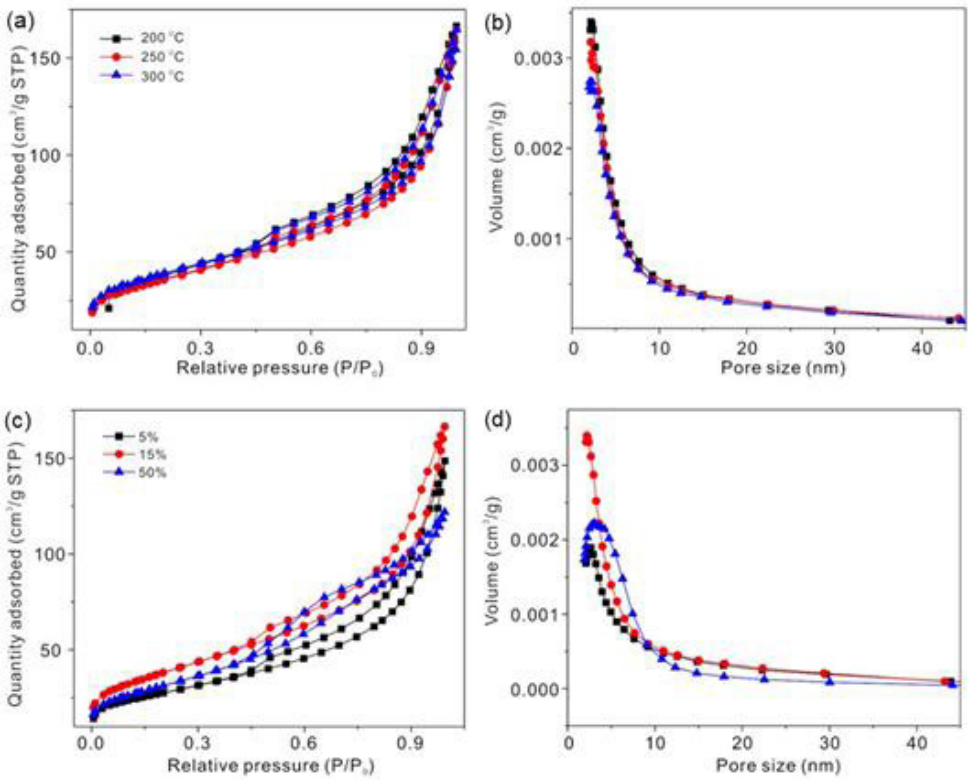

Fig. 7. (a) Nitrogen adsorption-desorption isotherms and (b) pore-size distribution of Fe-ATP prepared at different calcination temperatures, (c) nitrogen adsorption-desorption isotherms and (d) pore-size distribution of Fe-ATP with different iron contents.

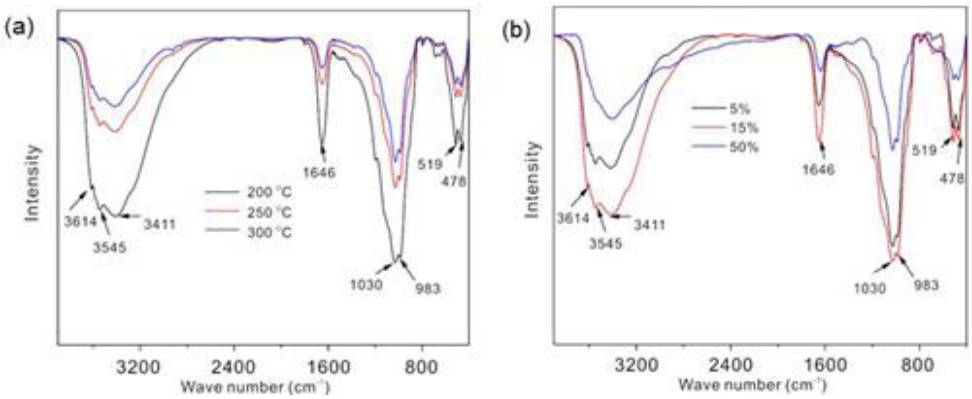

Fig. 8. FT-IR spectra of Fe-ATP prepared at different calcination temperature (a) and Fe-ATP with different iron contents (b).

first increased and then decreased. It also appears that with the more iron impregnated, an increasing fraction of pores in the ATP was blocked. Furthermore, the FT-IR measurements reveal that the –OH group intensity of the sample post-treated at 200°C with an iron content of 15% is superior to other samples (Fig. 8). As the sample calcinated at 200°C with an iron content of 15% has higher BET surface area and more functional groups, it has better adsorption performance than that of the samples calcinated at 250 and 300°C and with an iron content of 5 and 50%. In the following static adsorption and column studies the adsorbents used were those calcinated at 200°C with an iron loading of 15%.

Determined from the Langmuir equation, the maximum adsorption capacity for arsenite and arsenate by Fe-ATP was 23.47 and 6.74 mg/g at pH 7.0, respectively. The higher adsorption capacity for arsenite than for arsenate was also reported by other studies using iron oxides-based adsorbents [22,23]. Arsenic exists mostly in the form of As(III) under reducing conditions in groundwater [10]. The typical proportion of As(III) appears to be between 50–60% of the total arsenic in Bangladesh which is one of the most serious arsenic contaminated countries [22]. In addition, most of the reported adsorbents were not effective in As(III) removal compared with As(V), and the pre-oxidation of

As(III) to As(V) was usually needed. So, Fe-ATP is very favorable to treat groundwater without the need of pre-oxidation. In consideration of the adsorption capacity of arsenic, Fe-ATP appears to be much superior to most of other iron oxide-based adsorbents (Table 4) [24–30]. The higher arsenic adsorption capacity than the commonly reported adsorbents could be attributed to the high specific surface area of ATP clay and the high loading of iron.

3.3. Effects of pH on arsenic adsorption

The character of arsenic removal responding to pH variation has great significance in application. In addition, as the arsenic species and the surface charge of Fe-ATP in liquid phase depend on pH, the uptake of arsenic as a function of pH was investigated. Adsorption of arsenic in the pH range of 3–11 is shown in Fig. 9a. The removal efficiency of arsenate was higher than 99% in the pH range of 3–7. However, the percent removal of arsenate by Fe-ATP was reduced from 99.32% to 52.94% as the pH shifted from 7 to 11. In a wide pH range of 3–11, the removal efficiency of arsenite by Fe-ATP was higher than that of arsenate, which was in accordance with the results of adsorption isotherms. The percent removal of arsenite by Fe-ATP was above 93% except for pH 11. Although optimal As(V) removal was found in pH < 7 conditions, high removal performance was still observed near the neutral pH at a high initial concentration of As(V). As the pH value of natural water is in the range of 6–8.5, the pH pre-adjustment is not needed for the contaminated groundwater, considering the excellent performance of Fe-ATP in both As(III) and As(V) removal.

Fig. 9b presents the influence of the pH (3–11) on the zeta potentials of the adsorbent. The point of zero charge (pH_{PZC}) of the Fe-ATP is at about pH 8.45, which is in agreement with the iron oxides typically have PZCs in the range of 7–9 [22]. The surface of Fe-ATP is positively charged when the equilibrium pH values are below its pH_{PZC}. And the positively charged sites will be decreased with the increase of pH in solution. When the equilibrium pH increases to the value above pH_{PZC} of Fe-ATP, it will be negatively charged. The speciation of As(V) is pH dependent. H_3AsO_4 is the predominant species at pH below 2; $H_2AsO_4^-$ exists in the pH range of 2–7; $HAsO_4^{2-}$ exists in the pH range of 7–11; and AsO_4^{3-} is the major species at pH above 12. As the pH increased from 3 to 7, the main species of As(V) is monovalent $H_2AsO_4^-$ and multivalent $HAsO_4^{2-}$. And the mount of multivalent $HAsO_4^{2-}$ increased with the pH increased from 3–7. Although the pH was close to the pH_{PZC} of Fe-ATP, the multivalent $HAsO_4^{2-}$ increased either, and then the removal efficiency did not decrease in this case. As the equilibrium pH exceeded the pH_{PZC} of Fe-ATP, the surface sites were negatively charged which led to an increased repulsion to the negatively charged As(V) species. As a result, the adsorbed anionic As(V) species decreased on Fe-ATP at pH > pH_{PZC}. It is known that As(III) is stable as neutral H_3AsO_3 at pH < 9, while AsO_3^{3-}, $HAsO_3^{2-}$, and $H_2AsO_3^{2-}$ are the dominant species in the pH range of > 13, 12–13, and 9–12, respectively. Since the As(III) species have less negative charge character compared with As(V), As(III) was preferably adsorbed by Fe-ATP in a wide pH range. At lower pH values, the adsorption of neutral As(III) species and positively charged Fe-ATP can

Table 2
The data of specific surface area and pore size for the samples

Samples	S_{BET} (m^2/g)	V_{total} (cm^3/g)	Average pore size (nm)
200 °C-15%	137.6	0.225	6.54
250 °C-15%	128.8	0.209	6.48
300 °C-15%	137.8	0.217	6.31
200 °C-5%	98.9	0.192	7.75
200 °C-50%	113.5	0.171	6.01

Table 3
FTIR band positions and assignments for the samples

Frequency (cm^{-1})	Description
3614	υ(Mg, Al)OH
3545	υ(Fe^{3+}, Mg)OH
3411	Hydroxyl stretching vibration of coordinated water
1646	OH_2 bending vibration
1030	Si-O-Si stretching band
983	Si-O-Si stretching band
478	Si-O-Si deformation vibration

Table 4
Comparison on the As(III) and As(V) adsorption properties of various adsorbents

Adsorbents	As(V) Adsorption capacity (mg/g)	As(III) Adsorption capacity (mg/g)	Ref.
Iron-impregnated biochar	2.16	–	[24]
Humic acid coated magnetic iron oxide nanoparticles	12.6	12.2	[25]
Iron coated sand	–	0.075	[26]
Iron oxide amended rice husk char	0.95–1.46	–	[27]
Iron impregnated biochar	11.5	6.1	[28]
Iron/olivine composite	5.249	2.831	[29]
Iron modified Zeolite	0.05	0.1	[30]
Fe-ATP	6.74	23.47	This study

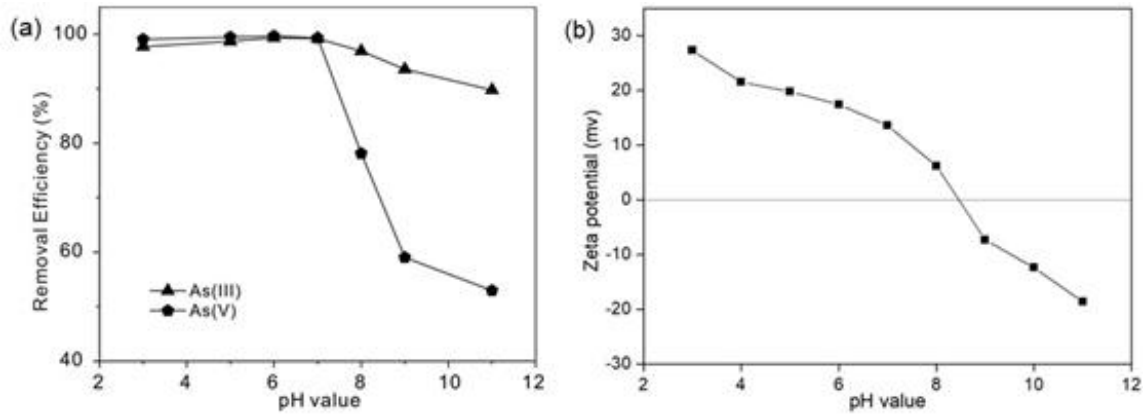

Fig. 9. Effects of pH on arsenic removal (a) and the zeta potential of the adsorbent (b).

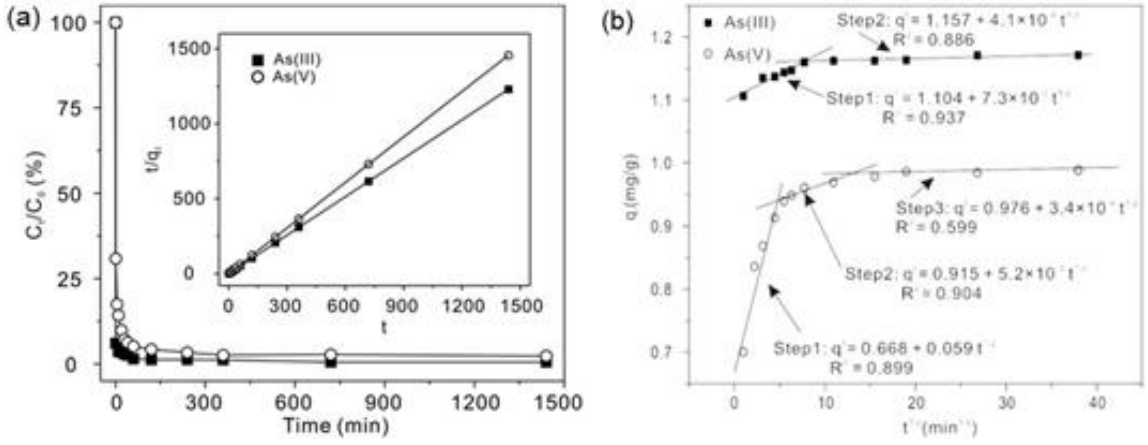

Fig. 10. (a) adsorption kinetics of arsenic on Fe-ATP at pH 7.0, inset is the corresponding pseudo-second-order kinetic model fitting. (b) Intraparticle diffusion model of arsenic on Fe-ATP at pH 7.0.

be attributed to the interaction of As(III) species with the surface –OH groups of Fe-ATP. The role of –OH groups in adsorption of As(III) by iron oxides have been reported by many researchers [31–33]. As pH increased, the amount of negatively charged As(III) species increased while the positively charged surface sites decrease up to pH_{PZC}. So the decrease in the adsorption efficiency at higher pH may be attributed to the negatively charged surface sites and an increase of negatively charged As(III) species. It is needed to point out that although the adsorption of As(V) was more sensitive to pH than As(III), the electrostatic adsorption is not the only adsorption mechanism of As(V) onto Fe-ATP. The interaction of As(V) with the surface –OH groups of iron oxides has also been reported [33].

3.4. Effects of contact time

The rate at which arsenic is removed from solution by the adsorbent is a significant factor for the utilization of the process in the treatment of effluents. The effect of contact time on the removal of arsenic by Fe-ATP is shown in Fig. 10a. As seen from Fig. 10a, the adsorption rate of As(III) and As(V) by Fe-ATP was very fast. The adsorption of As(III) and As(V) onto Fe-ATP was rapid for the first 1 h, when the elimination efficiency both reached 90% and then slowed down considerably. The adsorption kinetics results also showed that the higher removal efficiency of As(III) than that of As(V), which was consistent with the adsorption isotherm and pH tests. At the beginning, the adsorption rate was fast as arsenic was adsorbed by the exterior surface of the Fe-ATP adsorbents. When the adsorptions of the exterior surface reached saturation, arsenic entered into the pores of the adsorbent particles and was adsorbed by the interior surface of the particle. This phenomenon took a relatively long contact time.

The adsorption of a solute by an adsorbent in aqueous solution is often a phenomenon with complex kinetics. In order to investigate the adsorption processes of arsenic on the adsorbents, pseudo-second-order kinetic model was studied. The slope and intercept of plot of t/q_t vs. t were used to calculate the pseudo-second-order rate constant k_2 (inset in Fig. 10a). The values of pseudo-second-order parameters and correlation coefficients are presented in Table 5. The correlation coefficients of both examined data were found very high ($R^2 \geq 0.999$). This shows that the model can be applied for the entire adsorption process and confirms that the adsorption of arsenic on Fe-ATP followed the pseudo-second-order kinetic model. Table 5 also indi-

Table 5
Kinetic parameters for arsenic adsorption onto Fe-ATP

As species	q_e (mg/g)	k_2 (g/mg min^{-1})	R^2
Arsenite	1.17	0.97	0.999
Arsenate	0.99	0.62	0.999

cates that the rate constant k_2 of As(III) is 1.6 times that of As(V). However, the reason why the adsorption of As(III) was faster than As(V) by Fe-ATP is unclear.

To further study the adsorption kinetics of arsenic on Fe-ATP, a simplified intraparticle diffusion model was employed to elucidate the adsorption mechanisms. The intraparticle diffusion model is expressed by:

$$q_t = K_p t^{1/2} + c \quad (5)$$

where k_p is the intra-particle diffusion rate constant, in mg/g $h^{1/2}$, and C, in mg/g, is a constant related to the thickness of the boundary layer. It is generally found that the plot of q_t against $t^{1/2}$ may present a multilinearity, which indicates that two or more steps occur in the adsorption process. The first sharper portion is external surface adsorption; while the second portion is the gradual adsorption stage, where the intraparticle diffusion is rate-controlled. The third portion is the final equilibrium stage, where the intraparticle diffusion starts to slow down due to the extremely low solute concentration in solution. Fig. 10b shows the intraparticle diffusion results of arsenic adsorption on the Fe-ATP, which indicates that the As(III) adsorption on the Fe-ATP is in two stages. However, the As(V) adsorption on the Fe-ATP is in three stages.

3.5. Effect of co-existing anions

Natural groundwater always contains numerous aqueous constituents, which can compete for adsorption sites and decrease the removal efficiency of the adsorbent. Arsenic adsorption in the presence of potential co-existing anions was investigated, and the results are shown in Fig. 11. The removal efficiency for As(III) and As(V) by Fe-ATP was 99.5% and 98.1%, respectively, in the control adsorption tests with initial arsenic concentrations of 5.5 and 5.8 mg/L. It was observed that Cl^-, SO_4^{2-} and NO_3^- and HCO_3^- with concentrations up to 1 mM did not inhibit both As(III) and As(V) adsorption under the investigated conditions. This indicates that Fe-ATP had higher adsorption affinity for arsenic than for Cl^-, SO_4^{2-} and NO_3^- and HCO_3^-. PO_4^{3-} showed increasing levels of interference at increasing concentrations. As PO_4^{3-} concentrations increased from 0.1 to 1 mM, the removal efficiencies of As(III) and As(V) decreased from 98.1% and 80.4% to 87.1% and 14.3%, respectively. It is known that phosphorous and arsenic have very similar atomic structures and chemical properties. The phosphorous inhibition effects on arsenic adsorption have also been reported by others [22,34]. Considering the typical phosphate ranges in groundwater is 0–5 mg/L, the arsenic adsorption performance will be not influenced by the co-existing anions when Fe-ATP is used as adsorbents.

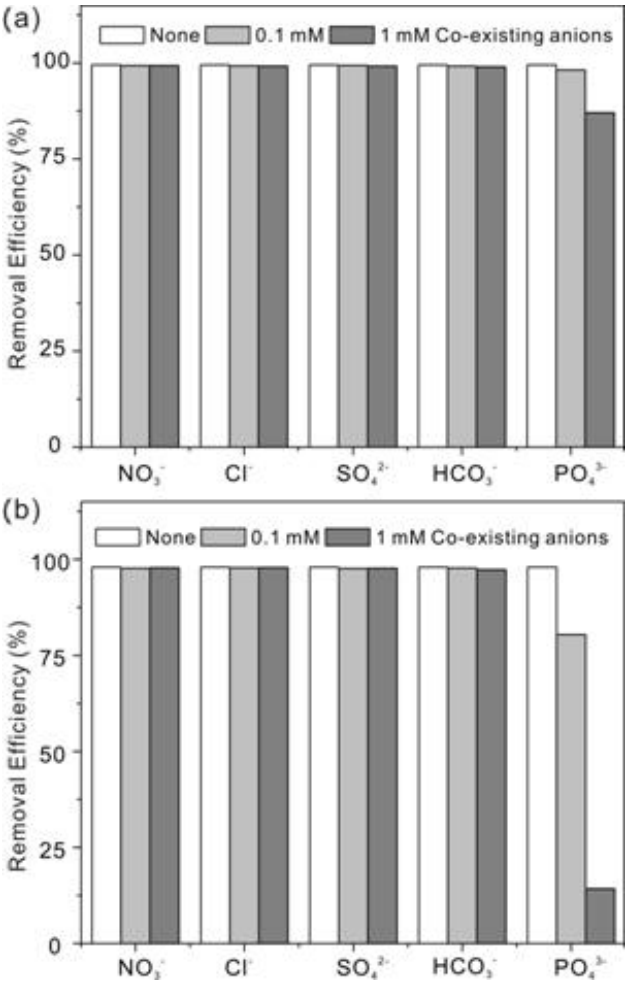

Fig. 11. Effects of co-existing anions on (a) arsenite and (b) arsenate removal.

3.6. Small-scale column study

Column tests were conducted to determine arsenic removal efficiencies for both lab-prepared arsenic-containing water and real groundwater contaminated by arsenic.

3.6.1. Synthetic arsenic-containing water

Fig. 12a shows complete effluent histories for As(III) during a fixed bed column run using Fe-ATP. With an influent As(III) concentration of 200 μg/L and pH of 7.0, about 4900, 1500 and 550 bed volumes (BVs) of lab-prepared water, respectively, corresponding to flowing rates of 200, 600 and 1000 mL/h, were treated before As(III) in the effluent reached 10 μg/L (WHO standard). While 50 μg/L (Bangladesh's arsenic maximum contaminant level (MCL)) As(III) breakthrough was observed after about 7300, 2950 and 1300 BVs when the flowing rate was 200, 600 and 1000 mL/h, respectively. Fig. 12b shows the As(V) removal capacities of Fe-ATP under the same conditions as the arsenite tests. For As(V) solution, at a flowing rate of 200 mL/h, Fe-ATP treated about 1320 and 2250 BVs and target concentrations of 10 and 50 μg/L, respectively. With increasing the

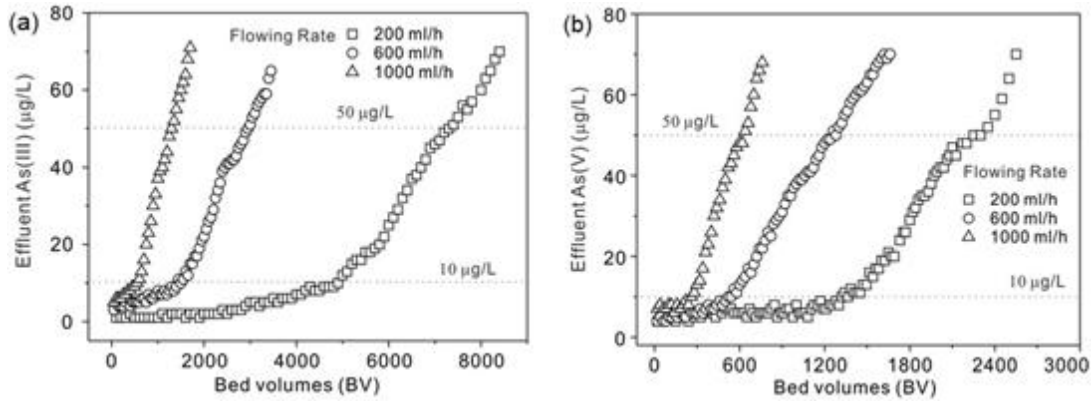

Fig. 12. Column tests of the Fe-ATP adsorbent in the treatment of lab-prepared As(III)-containing water (a) and As(V)-containing water (b). (Influent pH 7.0, influent [As] = 200 μg/L).

flowing rate to 600 mL/h, the As(V) concentration in the effluent solution was above 10 μg/L when the effluent volume reached 520 BVs, and achieved breakthrough at 1280 BVs when the As(V) effluent concentration was below 50 μg/L. About 260 and 640 BVs of As(V) solution were treated below 10 and 50 μg/L, respectively, by Fe-ATP at a flowing rate of 1000 mL/h. In previous adsorption isotherm study we have shown that the adsorption capacity of Fe-ATP for As(III) was about 3.5 times that for As(V) at neutral pH. Furthermore, the effluent concentrations of Fe and Al were analyzed in the present column tests. Very low concentrations of Fe (2 μg/L) and Al (5 μg/L) demonstrated that the prepared Fe-ATP was stable and safe. Therefore,from the column tests we can conclude that Fe-ATP showed higher removal performance for As(III) than for As(V), which was in accordance with the adsorption isotherm study. With higher removal performance for As(III), Fe-ATP is expected to be effective in treating groundwater in which As(III) is the dominant arsenic species.

3.6.2. Real arsenic-contaminated groundwater

To further examine the performance of Fe-ATP for a real groundwater, we used a real arsenic-contaminated groundwater from Togtoh Town, Inner Mongolia of China as the feeding solution and tested the enhanced arsenic removal performance by Fe-ATP. Table 6 shows the chemical analysis of the groundwater sample and the sample had a high arsenic concentration of 303 μg/L which is 30 times that of the MCL by WHO. Along with arsenic, the groundwater contains high concentrations of chloride (119.6 mg/L), sodium (395.2 mg/L), and TOC (22.23 mg/L). As expected, the results presented in Fig. 13 seem attractive for its practical application. Arsenic can be efficiently sequestrated by Fe-ATP within about 1300 BVs at the WHO provisional guideline value of 10 μg/L. According to the MCL of 50 μg/L in Bangladesh, breakthrough was observed at 2500 BVs. The better performance of Fe-ATP toward real groundwater can be attributed to the high percentage of As(III) (about 70%) in real groundwater. As the pH of the real groundwater is 8.52 and there are some interference anions and humic acid in it, the column performance was slightly poorer than the test for lab-prepared arsenic-containing water. Furthermore, the regeneration was con-

Table 6
Characteristics of groundwater from Togtoh Town, Inner Mongolia, China

Parameter	Value
pH	8.52
Total arsenic, mg/L	0.303
Total organic carbon, mg/L	22.23
Total hardness	0.108
Chloride, mg/L	119.6
Nitrate, mg/L	10.76
Sulfite, mg/L	4.74
Sodium, mg/L	395.2
Potassium, mg/L	2.46
Total iron, mg/L	0.25
Manganese, mg/L	0.02
Calcium, mg/L	3.24
Magnesium, mg/L	7.92
Zinc, mg/L	0.02
Alumina, mg/L	0.12

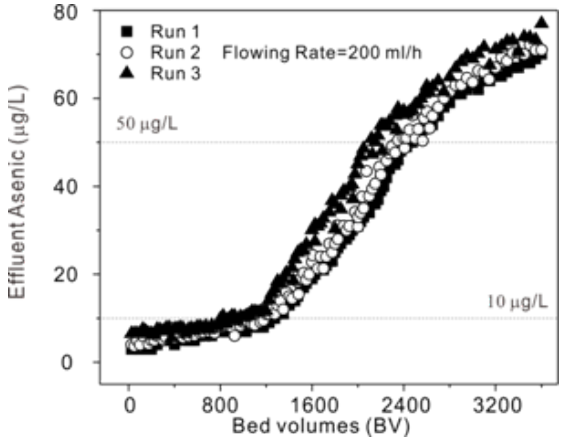

Fig. 13. Column tests of the Fe-ATP adsorbent in the treatment of real arsenic-contaminated groundwater for three recycles without adjusting the pH value.

ducted by shaking the exhausted Fe-ATP adsorbents in 0.1 M alkaline solution,which volume was about 1.5 times of the adsorbent, and the shaking time was 120 min. And then the regenerated Fe-ATP was eluted with deionized water for several times. After regeneration, more than 90% of adsorbed arsenic was removed from the adsorbents. As can be seen from Fig. 13, high arsenic removal performance was sustained in another two runs. After the first and second regeneration, the weights of the adsorbent were about 99.6% and 99.5% of the original value. A little of mass loss may be due to the shaking of the regeneration process and the cleaning of deionized water caused a small amount of powder flowing away with the water. The real groundwater trial demonstrated that the Fe-ATP can be used for treatment of arsenic-contaminated groundwater.

4. Conclusions

This research demonstrated that ATP is a suitable carrier for iron impregnation to create a more favorable iron based adsorbent for arsenic removal by controlling the iron content and calcination temperature. In batch tests, the maximum adsorption capacity for arsenite and arsenate by Fe-ATP was 23.47 and 6.74 mg/g at pH 7.0, which outperformed many other reported iron-impregnated adsorbents. The kinetic results revealed that both arsenite and arsenate adsorption onto Fe-ATP followed a pseudo-second-order kinetics model. In the near neutral pH, Fe-ATP showed higher removal efficiency for both As(III) and As(V). With the exception of PO_4^{3-} other co-existing anions had little effect on As(III) and As(V) removal by Fe-ATP when considering their typical concentration ranges in real groundwater. In column tests, Fe-ATP exhibited excellent performance for both lab-prepared and real arsenic-contaminated groundwater. In conclusion, this granular Fe-ATP adsorbent showed high application potential for arsenic removal from real groundwater, due to its high removal efficiency for both arsenite and arsenate. Further research is underway to evaluate the anti-striking, weight loss under flow flushing and backwashing and leaching toxicity of Fe-ATP adsorbents in long term column tests operation.

Acknowledgement

This work was supported by the National Natural Science Foundation of China (61873003, 21677001), the Natural Science Major Research Projects of Anhui Education Department (KJ2017ZD40, KJ2016SD14 and KJ2017ZD41), the Science and Technology Major projects of Anhui Province (16030801118, 18030801106 and 18030801104), the Scientific Research Start-up Foundation for Introduction of Talent, Anhui Jianzhu University (2016QD113), the Natural Science Research Project of the Higher Education Institutions of Anhui Province (KJ2016A143).

References

[1] H. Wang, X. Wang, J. Ma, P. Xia, J. Zhao, Removal of cadmium(II) from aqueous solution: A comparative study of raw attapulgite clay and a reusable waste–struvite/attapulgite obtained from nutrient-rich wastewater, J. Hazard. Mater., 329 (2017) 66–76.

[2] H. Yin, X. Yan, X. Gu, Evaluation of thermally-modified calcium-rich attapulgite as a low-cost substrate for rapid phosphorus removal in constructed wetlands, Water Res., 115 (2017) 329–338.

[3] Y. Tang, H. Zhang, X. Liu, D. Cai, H. Feng, C. Miao, X. Wang, Z. Wu, Z. Yu, Flocculation of harmful algal blooms by modified attapulgite and its safety evaluation, Water Res., 45 (2011) 2855–2862.

[4] X. Liu, R. Wang, Effective removal of hydrogen sulfide using 4A molecular sieve zeolite synthesized from attapulgite, J. Hazard. Mater., 326 (2017) 157–164.

[5] Y. Liu, W. Wang, A. Wang, Effect of dry grinding on the microstructure of palygorskite and adsorption efficiency for methylene blue, Powder Technol., 225 (2012) 124–129.

[6] D.Q. Pan, Q.H. Fan, P. Li, S.P. Liu, W.S. Wu, Sorption of Th(IV) on Na-bentonite: Effects of pH, ionic strength, humic substances and temperature, Chem. Eng. J., 172 (2011) 898–905.

[7] G. Zhang, Z. He, W. Xu, A low-cost and high efficient zirconium-modified-Na-attapulgite adsorbent for fluoride removal from aqueous solutions, Chem. Eng. J., 183 (2012) 315–324.

[8] H. Yin, M. Kong, W. Tang, Removal of fluoride from contaminated water using natural calcium-rich attapulgite as a low-cost adsorbent, Water Air Soil Pollut., 226 (2015) 425.

[9] X.Y. Yu, T. Luo, Y. Jia, Y.X. Zhang, J.H. Liu, X.J. Huang, Porous hierarchically micro-/nanostructured MgO: morphology control and their excellent performance in As(III) and As(V) removal, J. Phys. Chem. C, 115 (2011) 22242–22250.

[10] B.A. Manning, M.L. Hunt, C. Amrhein, J.A. Yarmoff, Arsenic(III) and arsenic(V) reactions with zerovalent iron corrosion products, Environ. Sci. Technol., 36 (2002) 5455–5461.

[11] Z. Cheng, F. Fu, D.D. Dionysiou, B. Tang, Adsorption, oxidation, and reduction behavior of arsenic in the removal of aqueous As(III) by mesoporous Fe/Al bimetallic particles, Water Res., 96 (2016) 22–31.

[12] X.Y. Yu, R.X. Xu, C. Gao, T. Luo, Y. Jia, J.H. Liu, X.J. Huang, Novel 3D hierarchical cotton-candy-like CuO: surfactant-free solvothermal synthesis and application in As(III) removal, ACS Appl. Mater. Interfaces, 4 (2012) 1954–1962.

[13] B. An, T.R. Steinwinder, D. Zhao, Selective removal of arsenate from drinking water using a polymeric ligand exchanger, Water Res., 39 (2005) 4993–5004.

[14] E. Deschamps, V.S. Ciminelli, W.H. Holl, Removal of As(III) and As(V) from water using a natural Fe and Mn enriched sample, Water Res., 39 (2005) 5212–5220.

[15] I.A. Katsoyiannis, A.I. Zouboulis, Removal of arsenic from contaminated water sources by sorption onto iron-oxide-coated polymeric materials, Water Res., 36 (2002) 5141–5155.

[16] Z. Lou, Z. Cao, J. Xu, X. Zhou, J. Zhu, X. Liu, S. Ali Baig, J. Zhou, X. Xu, Enhanced removal of As(III)/(V) from water by simultaneously supported and stabilized Fe-Mn binary oxide nanohybrids, Chem. Eng. J., 322 (2017) 710–721.

[17] X. Zhang, M. Wu, H. Dong, H. Li, B.-C. Pan, Simultaneous oxidation and sequestration of As (III) from water by using redox polymer-based Fe (III) oxide nanocomposite, Environ. Sci. Technol., 51 (2017) 6326–6334.

[18] X. Hu, Z. Ding, A.R. Zimmerman, S. Wang, B. Gao, Batch and column sorption of arsenic onto iron-impregnated biochar synthesized through hydrolysis, Water Res., 68 (2015) 206–216.

[19] S.K. Maji, Y.-H. Kao, C.-J. Wang, G.-S. Lu, J.-J. Wu, C.-W. Liu, Fixed bed adsorption of As(III) on iron-oxide-coated natural rock (IOCNR) and application to real arsenic-bearing groundwater, Chem. Eng. J., 203 (2012) 285–293.

[20] C. Nieto-Delgado, J.R. Rangel-Mendez, Anchorage of iron hydro (oxide) nanoparticles onto activated carbon to remove As (V) from water, Water Res., 46 (2012) 2973–2982.

[21] H. Yin, M. Kong, X. Gu, H. Chen, Removal of arsenic from water by porous charred granulated attapulgite-supported hydrated iron oxide in bath and column modes, J. Clean. Prod., 166 (2017) 88–97.

[22] X. Guo, F. Chen, Removal of arsenic by bead cellulose loaded with iron oxyhydroxide from groundwater, Environ. Sci. Technol., 39 (2005) 6808–6818.

[23] V. Lenoble, O. Bouras, V. Deluchat, B. Serpaud, J.C. Bollinger, Arsenic adsorption onto pillared clays and iron oxides, J. Colloid Interf. Sci., 255 (2002) 52–58.
[24] X. Hu, Z. H. Ding, A. R. Zimmerman, S.S. Wang ,B. Gao, Batch and column sorption of arsenic onto iron-impregnated biochar synthesized through hydrolysis, Water Res., 68 (2015) 206–216.
[25] M. Rashid, G.E. Sterbinsky, M.G. Pinilla, Y. Cai, K.E. O'Shea, Kinetic and mechanistic evaluation of inorganic arsenic species adsorption onto humic acid grafted magnetite nanoparticles, J. Phys. Chem. C , 122 (2018) 13540–13547.
[26] R.R. Devi, I.M. Umlong, B. Das, K. Borah, A.J. Thakur, P.K. Raul, S. Banerjee, L. Singh, Removal of iron and arsenic (III) from drinking water using iron oxide-coated sand and limestone, Appl. Water. Sci., 4 (2014) 175–182.
[27] C.O. Cope, D.S. Webster, D.A. Sabatini, Arsenate adsorption onto iron oxide amended rice husk char, Sci. Total Environ., 488–489 (2014) 554–561.
[28] M.E. Lee, P. Jeon, J.G. Kim, K. Baek, Adsorption characteristics of arsenic and phosphate onto iron impregnated biochar derived from anaerobic granular sludge, Korean J. Chem. Eng., 35 (2018) 1409–1413.
[29] P.S. Ghosal, K.V. Kattil, M.K. Yadav, A.K. Gupta, Adsorptive removal of arsenic by novel iron/olivine composite: Insights into preparation and adsorption process by response surface methodology and artificial neural network, J. Environ. Manage., 209 (2018) 176–187.
[30] Z.H. Li, J.S. Jean, W.T. Jiang, P.H. Chang, C.J. Chen, L.B. Liao, Removal of arsenic from water using Fe-exchanged natural zeolite, J. Hazard. Mater., 187 (2011) 318–323.
[31] G. Ona-Nguema, G. Morin, F. Juillot, G. Calas, G.E. Brown, Jr., EXAFS analysis of arsenite adsorption onto two-line ferrihydrite, hematite, goethite, and lepidocrocite, Environ. Sci. Technol., 39 (2005) 9147–9155.
[32] Z. Zhao, Y. Jia, L. Xu, S. Zhao, Adsorption and heterogeneous oxidation of As(III) on ferrihydrite, Water Res., 45 (2011) 6496–6504.
[33] G. Morin, G. Ona-Nguema, Y. Wang, N. Menguy, F. Juillot, O. Proux, F. Guyot, G. Calas, G.E. Brown, Jr., Extended X-ray absorption fine structure analysis of arsenite and arsenate adsorption on maghemite, Environ. Sci. Technol., 42 (2008) 2361–2366.
[34] H. Zeng, B. Fisher, D.E. Giammar, Individual and competitive adsorption of arsenate and phosphate to a high-surface-area iron oxide-based sorbent, Environ. Sci. Technol., 42 (2008) 147–152.